Approaches to partitioning the global UVER irradiance into its direct and diffuse components in Valencia, Spain

Manuel Nuñez,[1] M. Pilar Utrillas,[2] and Jose A. Martínez-Lozano[2]

Received 11 April 2011; revised 22 November 2011; accepted 23 November 2011; published 27 January 2012.

[1] The paper explores methods of partitioning the hourly average UV erythemal flux into its direct and diffuse components for Valencia, Spain. It is shown that the cloud modification factor, the ratio of measured to cloudless erythemal flux relates linearly to the fraction of the measured irradiance that is diffuse. This relationship was developed further into two simple models- a linear and nonlinear one. The models are characterized by an effective cloud cover to partition the global erythemal flux. The diffuse fraction increases linearly with cloud cover in the linear model, but exponentially in the nonlinear one. The models may be used to partition the direct and diffuse irradiance with RMS errors values ranging from 5.7 to 6.8 mWm^{-2} and 6.0–7.7 mWm^{-2} for direct and diffuse, respectively, with the nonlinear model performing best overall.

Citation: Nuñez, M., M. P. Utrillas, and J. A. Martínez-Lozano (2012), Approaches to partitioning the global UVER irradiance into its direct and diffuse components in Valencia, Spain, *J. Geophys. Res.*, *117*, D02204, doi:10.1029/2011JD016087.

1. Introduction

[2] Documented depletion of stratospheric ozone has spurred efforts to estimate the enhanced levels of ultraviolet radiation reaching the earth's surface and its potential impact on biological organisms [*Gao et al.*, 2010; *Zerefos and Bais*, 1995; *Trevini*, 1993]. Measurement networks encompassing different global environments have been established in the last two decades [see, e.g., *Bernhard et al.*, 2009; *Martínez-Lozano et al.*, 2002; *Steinmetz*, 1997; *Bigelow et al.*, 1998; *Kerr and Wardle*, 1993; *Roy et al.*, 1997]. Their instruments, typically measuring spectral or broadband UVA or UVB irradiance on a horizontal plane, provide much needed background data on the surface UV flux, its spatial and temporal change, and its response to a range of atmospheric and environmental factors. Partitioning these data into its direct and diffuse components is an important task for accurate estimates of biological impacts. In this paper we examine methods of estimating UV diffuse irradiance data (D) from global UV irradiance data (G) collected in Valencia, Spain with emphasis on cloud physical processes.

[3] In cloudless conditions radiative transfer models [*Mayer and Kylling*, 2005; *Kneizys et al.*, 1983; *Ricchiazzi et al.*, 1998; *Madronich and Flocke*, 1997] may be used to partition the global flux provided the necessary atmospheric input conditions are known. The task is however, much more complex in cloudy conditions given the variability in cloud structure and composition [*Nunez et al.*, 2005]. To date very few attempts have been made to partition the flux in cloudy conditions as the majority of studies have concentrated on UV global radiation transmission by clouds.

[4] A cloud modification factor (CMF_{UV}), commonly estimated as a ratio of measured to (usually) modeled cloudless global UV irradiance under the same conditions [*Calbo et al.*, 2005] has been linked to cloud cover and or cloud type and cover [*Esteve et al.*, 2010; *Renaud et al.*, 2000; *Thiel et al.*, 1997; *Josefsson and Landelius*, 2000; *Grant and Heisler*, 2000; *Foyo-Moreno et al.*, 2003; *Kuchinke and Nunez*, 1999]. Results show high variability in broadband cloud modification factors, (CMF_{BB}), even for constant cloud cover, providing evidence of cloud optical depths that are highly variable [*Renaud et al.*, 2000]. A strong dependence on cloud amount was obtained in all studies, as well as a dependence on cloud type [*Esteve et al.*, 2010; *Josefsson and Landelius*, 2000; *Kuchinke and Nunez*, 1999; *Thiel et al.*, 1997, *Grant and Heisler*, 2000]. Estimates differ even for the same cloud type, for example CMF_{UV} for low clouds and overcast conditions are reported as 0.25 [*Thiel et al.*, 1997], 0.35 (average) [*Josefsson and Landelius*, 2000], 0.52–0.56 [*Foyo-Moreno et al.*, 2003], 0.3–0.4 [*Kuchinke and Nunez*, 1999], and 0.4 [*Esteve et al.*, 2010].

[5] The above studies dealing with CMF_{UV} have been concerned with transmission of global UV irradiance. One exception is the work of *Grant and Gao* [2003] who examined the diffuse fraction of UVB radiation (k_{DUV}, ratio of measured diffuse to total global) as a function of total cloud cover and solar zenith angle. Using a modeling approach they related incremental changes in k_{DUV} (measured minus clear sky modeled k_{DUV}) to total cloud cover with encouraging results, obtaining a mean bias and RMS errors of 0.019 and 0.069 respectively. Even lower errors were obtained when added factors such as blockage of the solar beam are taken into account.

[6] In this study we wish to develop further the physical approach of *Grant and Gao* [2003] and apply it to the region

[1]School of Geography and Environmental Studies, University of Tasmania, Hobart, Tasmania, Australia.
[2]Solar Radiation Group, Departamento de Física de la Tierra, Universidad de Valencia, Valencia, Spain.

0148-0227/12/2011JD016087

of Valencia, Spain. We wish to concentrate on hourly averages as a compromise between high frequency stochastic processes of a few minutes duration and averages taken over several hours which will experience a range of zenith angles and possibly cloud types. Many stations do not record cloud observations and we will explore other radiation-based indices as surrogates for cloud cover. It is hoped that the methodology developed may be applied to provide diffuse irradiance data when only global data is available.

[7] Unless otherwise stated, references to global, diffuse and direct irradiance (G, D, and I respectively) in this text refer to erythemal global, diffuse and direct irradiance. Similarly CMF_{UV} and k_{DUV} refer to a cloud modification factor and diffuse to global fraction in the erythemal bands respectively. Root mean square errors are given in absolute units followed by their relative estimate (in brackets) obtained by dividing the RMS by the mean measured quantity.

2. Data Acquisition

2.1. Data Sources

[8] Measurements of UVER (UV erythemal radiation) were taken at the Burjassot campus of the University of Valencia (39° 30′N; 0° 25′W, 30 m) using two broadband YES-UVB-1 radiometers (Yankee Environmental Systems, YES), both located on the roof of the Faculty of Physics building, one measuring global irradiance on the horizontal plane and a second radiometer measuring diffuse irradiance using a shadow band.

[9] The YES-UVB-1 used to measure the global irradiance was calibrated in the National Institute for Aerospace Technology (INTA) at El Arenosillo, Spain. This standard calibration consists of a measurement of the spectral response of the radiometer indoors and a comparison with a Brewer MKIII spectroradiometer outdoors [*Vilaplana et al.*, 2006]. Using the LibRadtran model, correction factors are determined to transform the instrument signal, with its unique spectral response, into an erythemal response corresponding to the CIE action spectrum [*Commission Internationale de l'Eclairage* (*CIE*), 1998]. Second, an absolute calibration is obtained by an all-weather comparison with the MKIII spectroradiometer. The calibration matrix described by *Vilaplana et al.* [2006] provides errors that may arise in the calibration factor when no consideration is taken for variation in zenith angles. These are typically, a 9% error at zenith angle of 65 degrees, and increasing to 12% for a zenith angle of 70 degrees. With proper use of the calibration matrix, an overall uncertainty of 7% is expected in the measurement [*Gröbner et al.*, 2006]. All data was estimated using the calibration matrix, but at any rate, we restricted our data to zenith angles less than 70° given ancillary errors that could arise at high zenith angles (instrument leveling errors, azimuthal effects, etc.).

[10] A second radiometer measuring diffuse UVER with a shadow band has been calibrated by intercomparison with the first radiometer calibrated at INTA. Measurements of diffuse UVER using a shadow band have been corrected using the modified Batlles model proposed by *Utrillas et al.* [2007]. These corrected experimental values have an uncertainty estimated at 1%. Direct UVER on horizontal plane is obtained from the difference between measured global UVER and measured diffuse UVER on horizontal surface.

[11] Total column ozone data, used in model development was obtained from the OMI instrument aboard the Aura spacecraft. It is in a sun-synchronous orbit with a period of 100 min and providing world-wide coverage in spatial bins of 13 km × 24 km (http://aura.gsfc.nasa.gov/instrument/omi/index.html). Total column ozone data in 2004 was obtained from the TOMS instrument, OMI's predecessor. Data was downloaded from this website, one per day corresponding to days with UV measurements.

[12] Additional data consisted in 3 hourly total and low cloud observations for Valencia Airport (39°29′N; 0°28′W), expressed in oktas.

2.2. Data Measurement Period

[13] Data for two one year periods 2004 and 2007 were used in the analysis. These two years had good quality calibrated records for long periods as well as ancillary data on aerosol optical depth (AOD). UVER data was recorded as 5-min observations for both global and diffuse radiation using an Agilent 34970A data logger and were further processed to hourly averages for this analysis.

[14] A subset of data for 2007 was selected for cloudless conditions. This is a difficult process as there are no cloud images or cloud observations at the Burjassot site. As an alternative, three different procedures were followed to extract cloudless data. First, daily global irradiances were examined for each month and daily global above the 80 percentile levels were selected, on the supposition that the top 20% of daily global would represent cloudless conditions. A second approach involved calculating the lowest ratio of daily diffuse to daily global irradiance for a particular month. These ratios were ordered from lowest to highest and compared with the daily totals from the previous approach. Days selected with these two methods were also visually checked for irregularities in their plot which would denote cloudy conditions. The third step involved verifying that the selected days were cloudless or near-cloudless (2/10 of cloud amount or less as a daily average) with regards to cloud measurements at Valencia Airport, located approximately 5 km west of Burjassot. This analysis provided a total of 37 cloudless days for 2007 which included 402 h of direct and diffuse irradiance measurements.

3. Analysis

3.1. Cloudless Direct and Diffuse Irradiance

[15] Hourly UVER irradiance was produced using LibRadtran. LibRadtran (library for radiative transfer) is a collection of C and FORTRAN functions and programs for calculation of solar and thermal radiation in the Earth's atmosphere [*Mayer and Kylling*, 2005]. Its main tool is the UVSPEC (Ultra Violet Spectral) program (A. Kylling, UVSPEC User's Guide, 1995, available by anonymous ftp to ftp://kaja.gi.alaska.edu:/pub/arve (access March 2012)). It may be used to compute radiances, irradiances and actinic fluxes in the solar and terrestrial part of the spectrum. The UVSPEC model was run using the discreet ordinate method (DISORT) for a plane parallel atmosphere and in the six-stream mode. Model inputs are solar zenith angle at the mid-point of the hour considered, surface albedo taken as 0.05, a midlatitude summer atmosphere, total column ozone which scales the standard atmosphere by the total column amount, and an aerosol package consisting in aerosol optical depth and the single

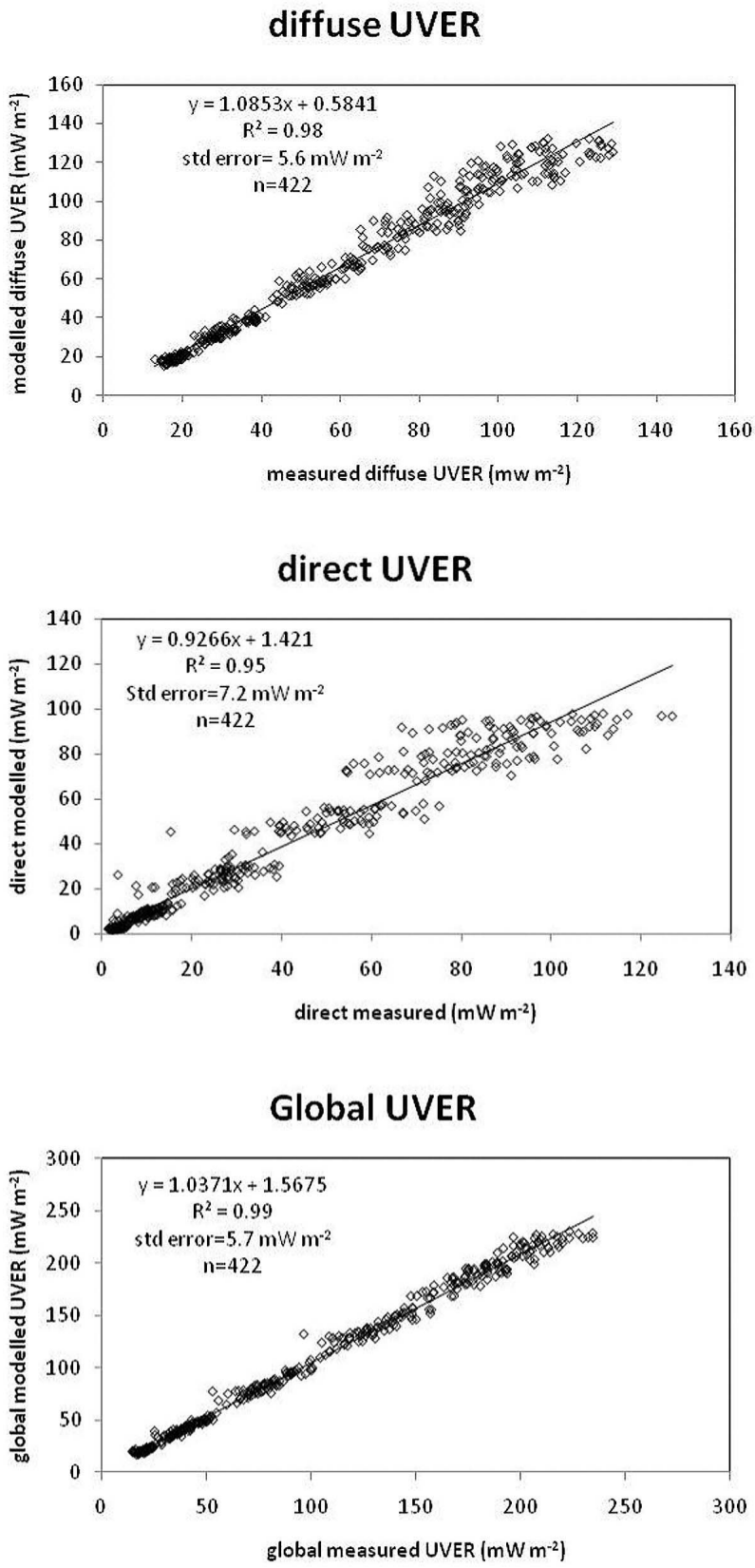

Figure 1. Comparison of UVSPEC model with measured data for Burjassot, Valencia. Data represents hourly cloudless irradiance for 2007.

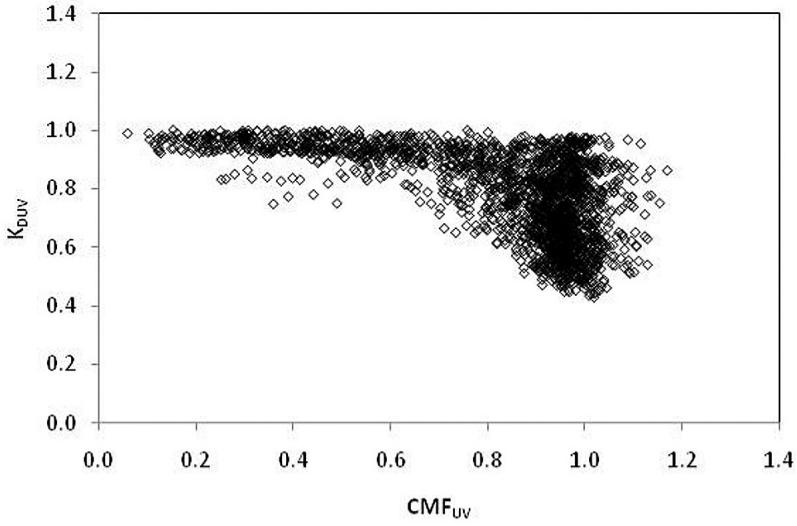

Figure 2. Plot of k_{DUV} versus CMF_{UV} for the Burjassot station. They encompass 2264 hourly records for 2007.

scattering albedo. Other aerosol parameters including vertical distribution and asymmetry parameters were covered by the default option which used the standard inputs of *Shettle* [1989].

[16] The design of UVSPEC allows simple problems to be easily solved using defaults and included data, hence making it suitable for educational purposes. At the same time the flexibility in how and what input may be specified makes it a powerful and versatile tool for research tasks. Input conditions consisted in total column ozone, AOD and aerosol single scattering albedo (SSA) for the selected cloudless days in 2007. While ozone data was obtained from OMI, there is no continuous AOD and SSA data for the UVER region covering the range of cloudless and cloudy days of this study. The model was run on hourly basis with a changing solar zenith angle used as input. Daily column ozone was used from the OMI instrument aboard the Aura spacecraft, while monthly averages of the single scattering albedo in the UV wavelengths were used from a previous study [*Nuñez et al.*, 2010]. Data from a Cimel sunphotometer operating at the experimental site in cloudless conditions provided continuous aerosol optical depth at six wavelengths in the visible and near infrared wavelengths. On an hourly basis the angstrom coefficients from the above data were used to estimate aerosol optical depth at 300 and 400 nm [see, e.g., *Pietruczuk and Jaroslawski*, 2008] and an average of these two optical depths were used as representative of the aerosol optical depth at the UV wavelengths. These hourly data were further averaged on a monthly basis, and used as a single input to the UVSPEC model, one value per month. The model was run as a batch job providing hourly global, diffuse and direct UV irradiance already convolved with the erythemal curve.

[17] Figure 1 presents the model performance. Errors in the estimate of global irradiance are lower than the estimate of its direct or diffuse component. An RMS error of 8 mWm^{-2} (8 percent) is obtained for the global irradiance parameterization, which is close to the lower boundary of aerosol-induced errors in the UVSPEC modeling trial listed by *Cordero et al.* [2007] Partitioning the global irradiance will introduce larger RMS errors of 8.5 mW m^{-2} and 6.0 mW m^{-2} (28 and 14 percent) for the direct and diffuse flux respectively. These are very likely caused by anomalous cloud contamination in the data set and as a result, an incorrect partitioning of the global flux by the shadow band assembly.

3.2. Cloud Modification Factor and the Diffuse Fraction

[18] Here we explore the relationships between CMF_{UV} and the diffuse fraction k_{DUV}. The justification is that any change in CMF_{UV} will affect k_{DUV} and must be related to a well-defined change in either cloud optical depth or cloud cover. At the two extreme ends (no cloud cover change or no changes in optical depth), a change in k_{DUV} would only result from a change in optical depth or cloud cover.

[19] Figure 2 shows a plot of all concurrent hourly k_{DUV} and CMF_{UV} for all data collected in 2007, a total of 2264 hourly records. There is much scatter in the data, although some prominent features appear. The diffuse fraction k_{DUV} is close to 1 at CMF_{UV} less than approximately 0.6. This feature is indicative of overcast conditions and the absence of direct radiation. Note that k_{DUV} data points do not follow unity as measurement errors are large in this CMF_{UV} range. A second feature is the considerable number of points that exhibit a value of CMF_{UV} exceeding unity. They are likely to represent measurements errors but some of the data may represent a real enhancement. This topic will be addressed later in this paper.

[20] The scatter masks a strong dependence on solar zenith angle, which may be observed by partitioning the data into 10 degree solar zenith angle bins and filtering out all CMF_{UV} which are less than 0.6, a rather arbitrary cut-off point below which k_{DUV} is one (Figure 3).

[21] Note the negative slope which are highly significant but decrease in absolute magnitude (tending to zero slope) as the solar zenith angle increases (Figure 3 and Table 1). The standard error in k_{DUV} does not vary much with zenith

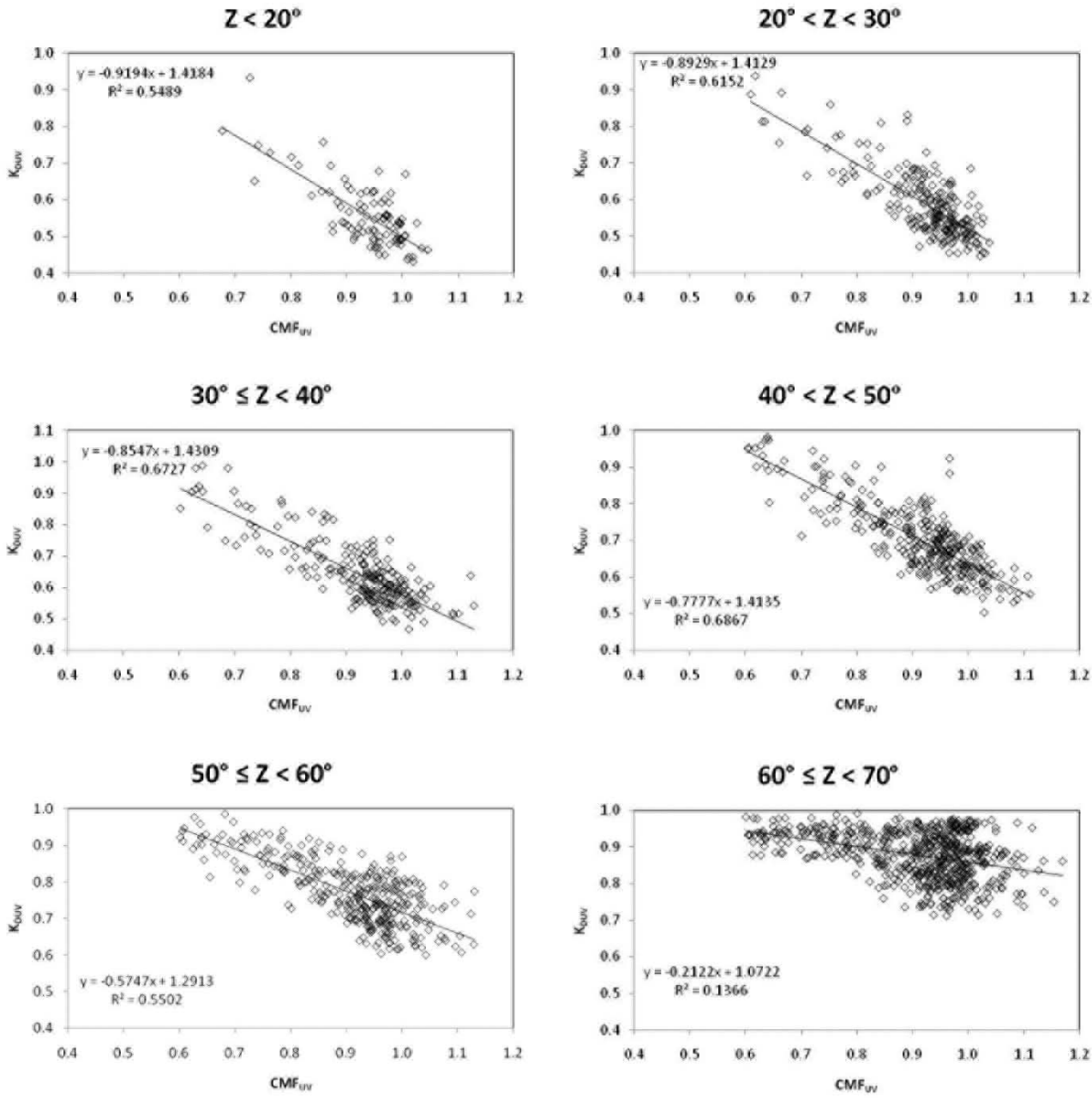

Figure 3. Scatterplot of k_{DUV} versus CMF_{UV} when grouped into 10 degree bins. Note a decreasing slope with increasing zenith angle.

angle, but more significant in terms of performance is the regression coefficient which decreases markedly with solar zenith angle. The low R^2 is likely to indicate measurement errors related to high solar zenith as will be discussed in the next section.

3.3. Estimation of Diffuse Fraction From Cloud Modification Factor Data

[22] Two different approaches to estimate k_{DUV} are described in this section. Their performances are assessed in the Results section.

3.3.1. Linear Model Using an Effective Cloud Cover

[23] The linear relationships between k_{DUV} and CMF_{UV} presented in Figure 3 argue that cloud structures organize themselves in a conservative fashion, at least with respect to the two indices, k_{DUV} and CMF_{UV}. In this section we consider a single cloud layer which covers a fraction C′ of the visible sky ranging from 0 to 1, and of uniform optical properties, e.g., uniform optical depth (effective cloud cover). By definition, the cloud model has two transmissions, a cloudless transmission equal to 1, and an "overcast transmission" which will depend on its optical depth, but is equal for all cloud portions.

Table 1. Statistics for Regression k_{DUV} = Slope * (CMF_{UV}) + Intercept[a]

Solar Zenith Angle (deg)	Slope	Intercept	R^2	Std Error	T Stat of Slope	n
<20	−0.919	1.42	0.55	0.059	−10.3	92
20–29	−0.893	1.42	0.62	0.057	−18.4	217
30–39	−0.855	1.43	0.69	0.058	−21.7	216
40–49	−0.777	1. 41	0.68	0.054	−25.6	304
50–59	−0.574	1.29	0.55	0.057	−20.7	349
60–69	−0.216	1.07	0.14	0.060	−9.9	610

[a]Here k_{DUV} is the diffuse fraction formed by dividing hourly measured diffuse irradiance by the corresponding measured global irradiance. CMF_{UV} is the ratio of measured to clear sky model global irradiance. Data was collected in 2007 and has been grouped into 10 degree solar zenith angle bins.

It is then possible to describe the hourly irradiance as a sum encompassing the portion of the sky that is cloudless $(1 - C')G_0$, plus that portion which is overcast, $C'G_0T_C$, where C′ is the effective cloud cover, T_C is an overcast transmission which remains constant and G_0 is a cloudless sky global irradiance:

$$G = (1 - C')G_0 + G_0T_CC' \tag{1a}$$

$$G = [(1 - C')I_0] + [(1 - C')D_0 + G_0C'T_C] \tag{1b}$$

where G, I and D represent global, direct and diffuse irradiance respectively, subscript "0" represents cloudless conditions and C′ is an effective cloud cover. The direct and diffuse irradiance are contained in the first and second terms in the square bracket. The terms k_{DUV}, CMF_{UV} and C may be readily obtained as:

$$k_{DUV} = \frac{(1 - C')D_0 + G_0C'T_C}{(1 - C')G_0 + G_0C'T_C} \tag{2}$$

$$CMF_{UV} = 1 + C'(T_C - 1) \tag{3}$$

$$C' = \frac{1 - G/G_0}{1 - T_C} \tag{4}$$

Therefore estimates of k_{DUV} in equation (2) depend explicitly on cloudless diffuse and global irradiance (D_0, G_0), effective cloud cover C′ and an overcast transmission T_C. As C′ depends also on T_C (equation (4)), the predictive ability of the model depends on how valid is the assumption of a constant T_C for a range of conditions.

[24] From Figure 2, it is also possible to define an "overcast transmission" as the value where k_{DUV} reaches 1 and CMF_{UV} is less than or equal to 0.6. Examining all data points that met this condition and grouping them according to zenith angle ranges, we arrive at the statistics of Table 2. With the exception of the high zenith angle regression (>60°), all average transmissions are within one standard error (Table 2). Therefore the overcast transmission in the analysis was taken as constant and with a value 0.495, the average of the five regressions with a zenith angle less than 60 degrees. Hourly k_{DUV} may be estimated by first solving equation (4) for C′ and then solving equation (2).

[25] To summarize, effective cloud cover C′ is related to a measured transmission $(1 - G/G_0)$ expressed as a fraction of the overcast value $(1 - T_C)$. However, it is important to note that C′ may take values that less than zero and greater than one, the first case when there is global irradiance enhancement above the cloudless sky by cloud lensing effects as discussed previously. The ratio G/G_0 decreases to values less than 0.5 when C′ is greater than one, until eventually C′ equals 2 when there is no measured global irradiance.

3.3.2. Nonlinear Model Using an Effective Cloud Cover

[26] Here we relax the condition that the cloud layer has uniform optical properties with cloud cover. Increasing cloud cover may manifest itself as a thicker cloud layer with higher liquid water and consequently, lower transmission, essentially describing a nonlinear behavior in a transmission versus cloud cover plots. To explore this effect we examine the ratio of direct measured to direct model (I/I_0) and diffuse measured to diffuse model (D/D_0) irradiances, with the model irradiances being cloudless and already defined in equation (1). Hourly data for 2007 data were selected containing concurrent measurements and model calculations and with the added filter that only solar zenith angles less than 60 degrees were considered. Measurement errors at higher zenith angles introduce distortions to the trends and confuse information on the relevant physical processes. As the diffuse fraction is close to one at these angles, it is unlikely that neglecting these data will be important. As in the linear model, we estimate an enhanced cloud C′ by the use of equation (4), which relates a measured to an overcast transmission $(1 - G/G_0)/(1 - 0.495)$.

[27] Figure 4 presents hourly plots of $\ln(I/I_0)$, I/I_0 and D/D_0 versus effective cloud cover for 2007. Note the strongly linear behavior of $\ln(I/I_0)$ versus C′ (Figure 4a), suggesting that the relationship between I/I0 is exponential and as verified in Figure 4b. It is also interesting to note that there are occasions when C′ exceeds one in Figures 4a–4c, representing a region where there is strong depletion when all global radiation is already diffuse, a region characterized by increasing optical depth of an already overcast sky. At C′ equal to 2 there is no global irradiance as may be noted from the definition of C′ and T_c.

[28] At the other extreme C′ is negative, indicating increased global irradiance above the cloudless value, very likely induced by scattered cloud effects. The behavior of the normalized diffuse irradiance, Figure 4c, is substantially different from that of the direct irradiance. From C′ equal to 0 to 1 there is no depletion of diffuse irradiance as D_0 is being fed by scattered direct irradiance from the cloud field. All direct irradiance is depleted above C′ equal to 1 and in this region D/D_0 starts to

Table 2. Statistics for Overcast Transmission, Defined as the Value Where CMF_{UV} Equals or is Less Than 0.6

Zenith Angle Range (deg)	Overcast Transmission
<20	0.456 (0.340–0.533)
20–29	0.461 (0.404–0.506)
30–39	0.514 (0.548–0.473)
40–49	0.533 (0.559–0.500)
50–59	0.511 (0.545–0.467)
>60	0.349 (0.442–0.208)

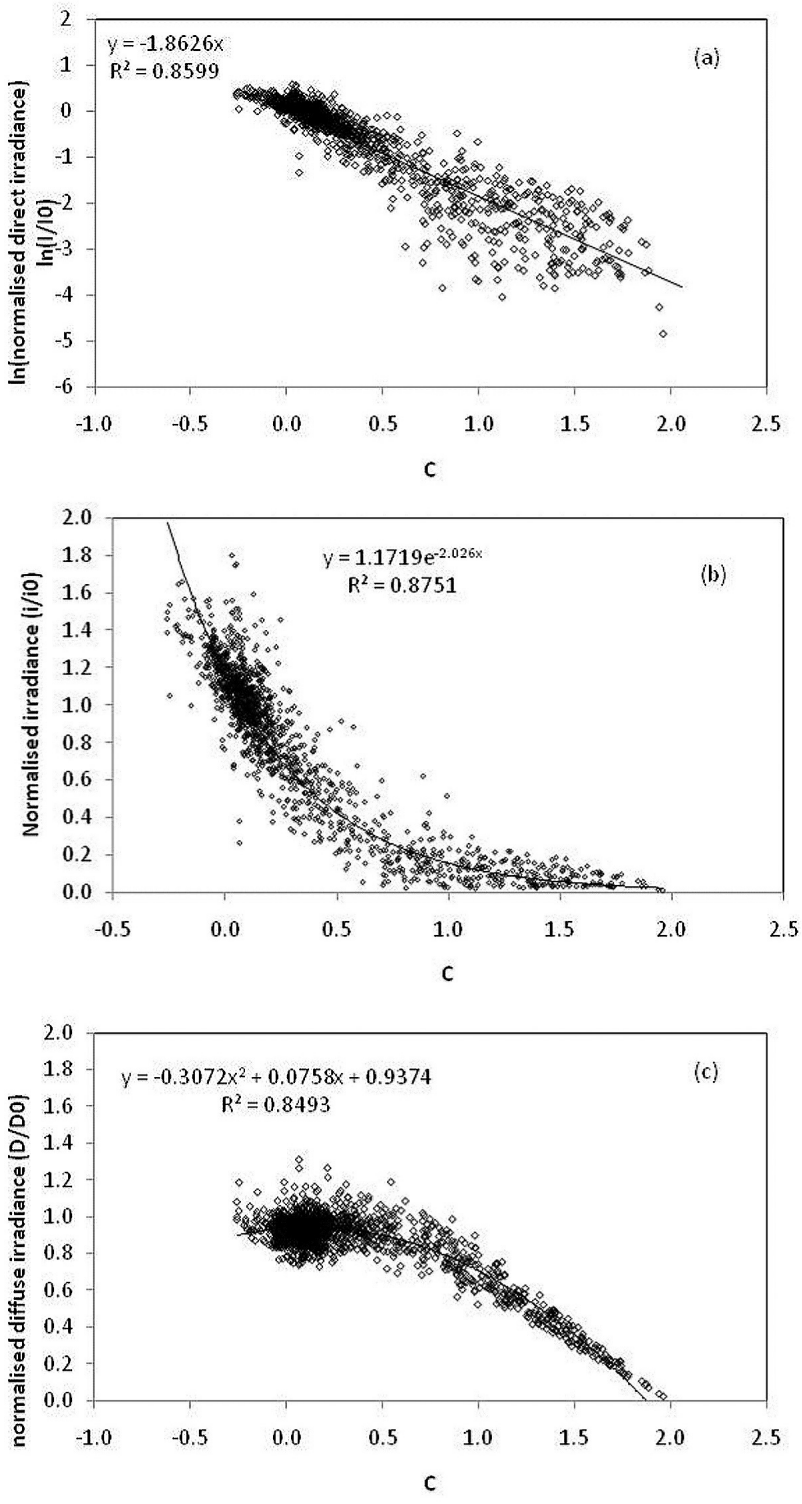

Figure 4. Scatterplot of (a) log normalized direct irradiance [$\ln(I/I_0)$] versus effective cloud cover C, (b) normalized direct irradiance (I/I_0) versus effective cloud cover C′, and (c) normalized diffuse irradiance (D/D_0) versus effective cloud cover C′. Hourly data for 2007 has been used.

Table 3. Model Performance of Two Models Used to Partition Global Irradiance[a]

		Direct	Diffuse	K_{DUV}
Linear Model	R^2	0.95	0.96	0.84
	RMS	6.8	7.7	0.06
	MBE	−2.3	−2.4	0.03
Non-linear model	R^2	0.96	0.97	0.84
	RMS	5.7	6.0	0.05
	MBE	−1.3	1.3	0.01

[a]Statistics are based on 2020 hourly measurements collected in 2004.

decrease, a result of increasing optical depth of the cloud. Finally at C′ equal to 2, all measured diffuse irradiance is zero.

[29] The nonlinear behavior of I/I0 and D/D_0 versus C′ described in Figure 4 will be used as predictive tools with an independent data set. Explicitly they may be written as:

$$\frac{I}{I_0} = 1.1719\exp(-2.026C'); \; R^2 = 0.87; \; n = 1448 \tag{5a}$$

$$\frac{D}{D_0} = 0.0344\,C'^3 - 0.385\,C'^2 + 0.1153C' + 0.9355; \quad R^2 = 0.85; \; n = 1448 \tag{5b}$$

and therefore only rely on C′ as the independent variable.

4. Results

[30] The above two models were tested against independent measurements of direct and diffuse fluxes for 2004 taken ant at the Burjassot campus of the University of Valencia. In total there were 2020 hourly measurements available for comparison encompassing the months of May to December. In a predictive mode, the linear model described in equations (1) to (5) has to be adjusted for extreme values in C′ when it becomes negative or greater than 1. By definition direct radiation becomes zero with C′ greater than one, and at the other extreme, it is set equal to the cloudless direct irradiance I_0 when C′ becomes negative, the assumption being that all added global irradiance is diffuse.

[31] Table 3 describes the results. The above two models predict direct and diffuse irradiance with a regression coefficient equal to or above 0.95. Root mean square errors for absolute direct irradiances are 6.8 mWm^{-2} (29 percent of the mean) for the linear model versus 5.7 mWm^{-2} (25 percent of the mean) for the nonlinear one. Absolute errors for diffuse irradiance are higher with the linear model registering 7.7 mWm^{-2} (13 percent of the mean) versus 6.0 mWm^{-2} (11 percent of the mean) for the nonlinear one. Correlations are lower for k_{DUV} as expected since errors are additive in the division process. The three statistical criteria (R^2, RMS and MBE) and three fluxes (direct, diffuse and k_{DUV}) make a total of nine indicators of goodness of fit. Of these nine, the nonlinear model scored highest on eight occasions and tied with the linear model on one occasion.

[32] Figures 5a–5d presents plots of the linear and nonlinear models versus measurements. There are systematic differences introduced by the linear model. There is a distinct nonlinearity in the estimates of direct irradiance using the linear model, which may be seen by model over-prediction at high irradiances. There are also some artificial features being introduced by the condition that model irradiances equal the cloudless values when C′ is less than zero. This nonlinearity is also evident in the k_{DUV} graph for the linear model. These features are lacking in the nonlinear model, which also explains the lowest mean bias error reported for the nonlinear model in Table 3.

5. Analysis Errors

[33] As discussed earlier, the calibration uncertainty for the global UVER measurement is around 7% for zenith angles less than 70°. Model errors must be added as well for the estimation of CMF_{UV}. Errors in the UVSPEC model can be considerable and arise mainly due to incorrect estimation of the aerosol and ozone column parameterization [*Cordero et al.*, 2007]. Typical errors in the OMI-TOMS parameterization when checked with Brewer estimates are around 1% when averaged on a global basis [*McPeters et al.*, 2008; *Balis et al.*, 2007] which agrees with comparisons done in southern Spain [*Anton et al.*, 2010]. Use of a monthly aerosol optical depth in the model can give rise to RMS errors of 64% in the estimation of daily aerosol optical depth. Substituting these error figures in the UVSPEC code with average conditions give rise to a total RMS error of 7.4% in estimating the clear sky irradiance.

[34] Using propagation of errors with quadratures [*Young*, 1963] we can estimate the error in CMF_{UV} as arising from errors in the measured and modeled clear sky irradiance [G, G_0], the errors in diffuse irradiance as errors in the global irradiance with and without the shadowband [G, G′], and the diffuse fraction as errors in the diffuse and global measured [D, G]. According to quadrature theory, errors in the function F when the component X, Y are dividing or adding may be written as equations (6) and (7) respectively:

$$\frac{\delta F}{F} = \left[\left[\frac{\delta X}{X}\right]^2 + \left[\frac{\delta Y}{Y}\right]^2\right]^{1/2} \tag{6}$$

$$\frac{\delta F}{F} = \frac{[(\delta X)^2 + (\delta Y)^2]^{1/2}}{X + Y} \tag{7}$$

Equation (6) was employed to estimate in CMF_{UV} and k_{DUV}, and equation (7) was used for D. Substituting the errors listed in G and G_0, we arrive at errors of 10.2%, 9.9% and 14.4% for CMF_{UV}, D and k_{DUV} respectively. It is also relevant to note that the above relationships assume that the data sets X,Y are independent of each other.

[35] Instrument errors represent the inherent uncertainty in the experimental determination of CMF_{UV}, D and k_{DUV}. Measurement errors also feed into the linear and nonlinear

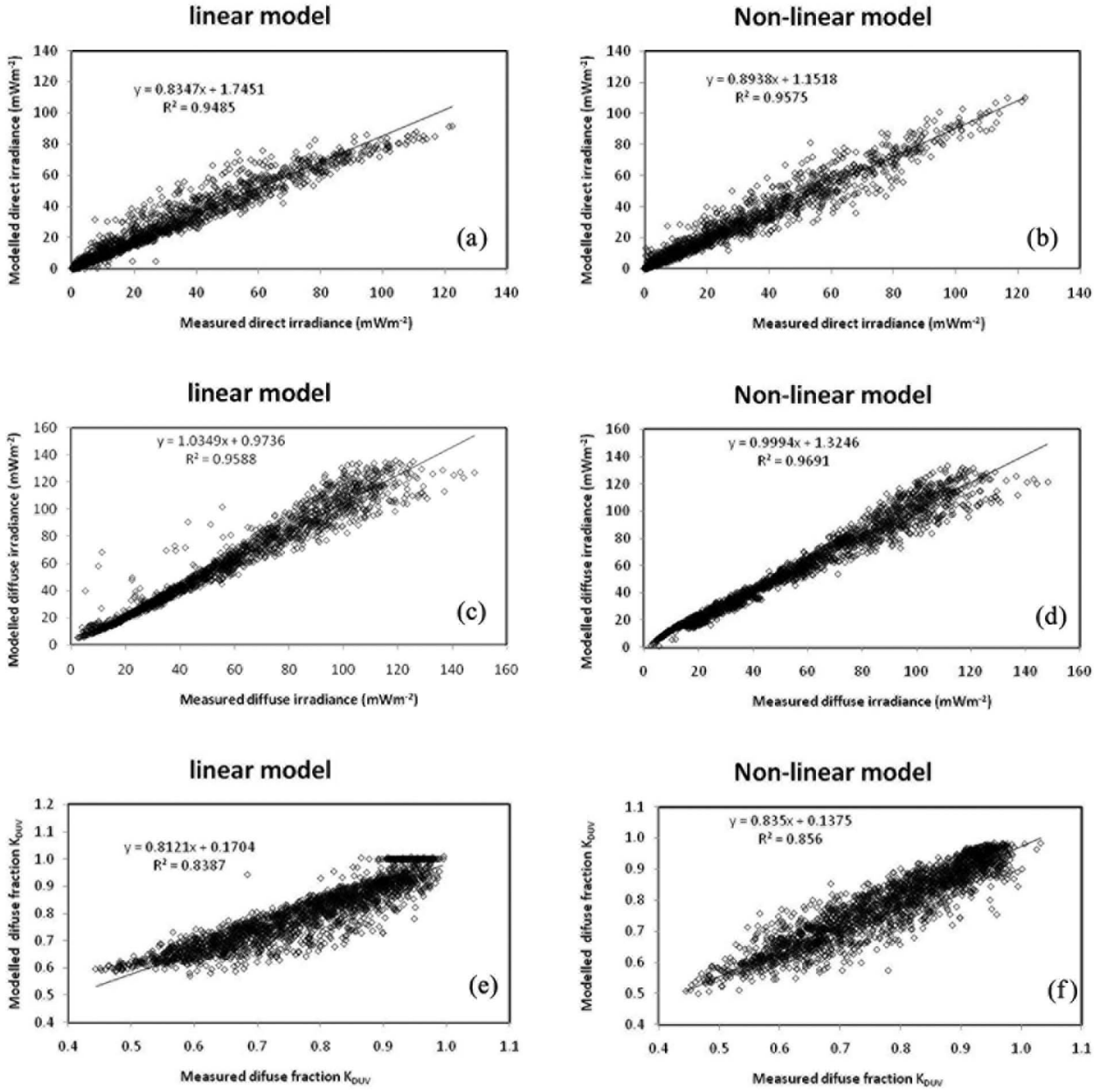

Figure 5. Modeled versus measured (a) direct irradiance for linear model, (b) diffuse irradiance for linear model, (c) direct irradiance for nonlinear model, (d) diffuse irradiance for nonlinear model, (e) diffuse fraction (k_{DUV}) for linear model, and (f) diffuse fraction (k_{DUV}) for non-linear model.

models described in Figure 5 and Table 3 which estimate I, D and k_{DUV} using mainly measured and clear sky global irradiance (G, G_0 respectively). As a result, model estimates of I, D and k_{DUV} contain both errors in the input variables and errors incurred by the model methodology and assumptions. As both measured and modeled data sets use measurements that contain some errors, the results in Figure 5 and Table 3 do not describe the departure from the true estimates of I, D and k_{DUV} but rather the agreement between the measured and modeled data sets.

[36] Table 4 summarizes all the error and uncertainties collected in the study. The second column describes the measurement errors (in mW m^{-2}) obtained by taking the product of the instrument error (in percentages) times the average I, D, and k_{DUV} of the 2004 measured data. Columns 3 and 4 are the RMS differences between measured and modeled data for the linear and nonlinear model respectively. Both the linear and nonlinear models estimate I with a higher RMS uncertainty compared to the inherent instrumental error. This is likely due to model assumptions involving direct radiation. RMS differences in estimating D are approximately similar to the instrumental error, while RMS differences in estimating k_{DUV} are lower than the instrumental error. The results for k_{DUV} are interesting as

Table 4. Summary of All Errors and Uncertainties[a]

	Instrumental Measurements RMS Error (mW m^{-2})	Linear Model RMS Difference (Measured – Model) (mW m^{-2})	Nonlinear Model RMS Difference (Measured – Model) (mW m^{-2})
Direct irradiance	3.4 (7.0%)	6.8	5.7
Diffuse Irradiance	8.1 (9.9%)	7.7	6.0
k_{DUV}	0.11 (14.4%)	0.06	0.05

[a]Instrumental errors use quadrature theory and are described in the second column. RMS errors between model and measurements are described in the third and fourth columns.

they illustrate differences between instrumental errors and model uncertainty. The instrumental errors in estimating k_{DUV} use quadrature theory and independent measurements of G and D (equation (6)). However, G and D are negatively correlated which in turn will lower the uncertainty between measured and modeled k_{DUV}.

[37] Averaging experimental data over a number of measurements will lower the overall error provided that there is no systematic error and the errors are random. This topic will be described further in the Discussion section which examines episodes in which CMF_{UV} is larger than 1.

6. Discussion

[38] Modeling the fraction of global radiation that is diffuse has relied on cloud cover as an index of atmospheric opacity [*Grant and Gao*, 2003]. However, cloud observations are laborious to obtain and are in most cases only available at meteorological stations. As an alternative, CMF_{UV} is developed here as an index of atmospheric opacity. We show that there is a well defined relationship between the fraction of global radiation at the surface that is diffuse (k_{DUV}) and CMF_{UV}. These results argue for well-structured cloud systems that have clear radiative signal, at least at the hourly scale.

[39] Two relationships have been developed to describe the partitioning of the global flux, a linear model with a single cloud optical depth and a nonlinear model describing increasing optical depth with cloud cover. A feature of the relationships is that they use an effective cloud cover, developed from CMF_{UV} measurements but with the added property that it may be negative, indicating enhanced fluxes above the clear sky, and also reach values above 1, indicating increasingly stronger depletion of radiation reaching the ground.

[40] The linear model described in this study rests on the concept that there is an "overcast" CMF_{UV}, mainly 0.495, below which all radiation is diffuse and above which there is some direct radiation. These figures are higher than the CMF_{UV} reported for low clouds in the literature and lower than equivalent figures for high clouds [*Esteve et al.*, 2010; *Josefsson and Landelius*, 2000; *Kuchinke and Nunez*, 1999; *Thiel et al.*, 1997; *Grant and Heisler*, 2000; *Foyo-Moreno et al.*, 2003]. Average CMF_{UV} shows a high variability [*Calbo et al.*, 2005] and it is likely that our overcast estimates of 0.495 are based on the presence of multiple cloud layers.

[41] Analysis of the 2007 data revealed that the relationship between CMF_{UV} and cloud cover is nonlinear for both direct and diffuse normalized irradiance. Best estimates of the fluxes and k_{DUV} were obtained when these nonlinear relationships were used as predictive tools to estimate irradiance and k_{DUV} for the 2004 data. They are, nevertheless, empirical relationships based on measured data for one specific year. More detailed studies using added ancillary data, such as for example cloud type and cloud observations would provide means to extend the relationships into a more general physical model applicable to other locations.

[42] Of interest to this study is the degree that global irradiance is enhanced above the clear sky value in cloudy conditions. Figure 2 argues that, despite the importance of instrumental errors, the effect could be real. To observe a potential cloud enhancement we first removed all cloudless days from the analysis, which left a total of 1762 hourly measurements for 2007. Of these, 152 h had a CMF_{UV} which exceeded 1, which made a total of 8.8% of the observations with an average CMF_{UV} of 1.029.

[43] We next develop a statistical test to examine the validity of this enhancement as shown in Table 5. This average CMF_{UV} is considered not significant if the (lower) range traced by two standard deviations in the measurement error of CMF_{UV} reaches a value less than one. If the low end of the range were to be below 1, there is a 5 percent possibility that the average measurement which is greater than 1, is a result of chance. Results from Table 5 indicate that the 95 percentile range in CMF_{UV} is above 1 and therefore that some of the high CMF_{UV} ratios are real.

[44] Enhancing of CMF_{UV} described in the literature in most cases apply to shorter time periods than one hour. *Sabburg and Wong* [2000] report that 8 percent of CMF_{UV} measurements are over 1 when 15 min measurement averages are used. *Mims and Frederick* [1994] measured a 16.5 percent enhancement over a 34 min period and *Segal and Davis* [1992] describe enhancements of 10–20 percent in CMF_{BB} over 15–30 min. Even at shorter averaging periods of 3 min, *Schafer et al.* [1996] report enhancements of up to

Table 5. Error Analysis for All CMF_{UV} Larger Than 1 Using Only Days That Were Not Classified as Cloudless[a]

Total Data Points	(N) Total Points With CMF > 1	Average CMF_{UV} Above 1	Measurement Error (18%)	±2 Error/SQRT(N)	Range for 95% Level of Confidence
1762	155	1.029	0.18	±0.014	1.01–1.04

[a]Given a mean figure of 1.029 for all CMFUV above 1, the likely 95 percent level of confidence range is from 1.01 to 1.04. Therefore it is likely that this average above 1 is real.

11 percent. Over hourly periods, *Foyo-Moreno et al.* [2003] document long-term averages that exceeded 1 for low to middle cloud cover and high zenith angle.

[45] Figure 4b provides further information on enhancement in partly cloudy conditions. At negative C′ (CMF_{UV} greater than 1), direct normal irradiance continues to increase but diffuse irradiance (Figure 4c) does not increase on average. Therefore most of the increase in global irradiance is driven by direct radiation. This conclusion warrants an examination of how direct irradiance is obtained, especially in cloudy conditions. It may be written as:

$$I = G - D \tag{8}$$

[46] While G measures irradiance from the entire sky, D by means of the shadow band filters out direct irradiance. The process is very effective for clear skies but partly cloudy skies create situations where a large amount of scattering occurs close to the solar beam [*Weihs et al.*, 2000; *Sabburg and Wong*, 2000]. Any increase in irradiance above the clear sky value is readily picked up by the pyranometer (G), but the shadowband instrument will not sense it if much of the increased scattering follows the direct beam.

[47] Enhancement in I will depend on the geometry of the shadowband which follow established guidelines [*Utrillas et al.*, 2007]. In our case the shadow band provides an obstruction of ±5.5 degrees along the plane of the solar beam. Pyrheliometers are designed to measure irradiance from a solar beam centered on the sun which includes circumsolar irradiance (B. W. Forgan, personal communication, 2010). To be consistent with these measurements, shadowband assemblies should block most of the circumsolar radiation, with this term appearing as part of the direct radiation which is estimated as a residual (equation (6)). *McArthur* [2004] lists typical shading disk geometries which should subtend a five degree full angle from the center of the detector in the Baseline Surface Radiation Network Programme, considerably smaller than the 11 degrees full angle that we used. However, a figure of 11 degrees blocking appears effective when navigation errors and other geometry errors are added to the total uncertainties involved in the measurement [*McArthur*, 2004; *Major*, 1992]. We conclude by stating that circumsolar radiation is likely to be dominant in the cloud enhancement of global radiation.

7. Conclusion

[48] The study has examined two techniques to partition global UVER into its diffuse and direct components. The first technique uses a simple model which partitions global irradiance into direct and diffuse irradiance in a linear fashion. The second approach develops empirical expressions for diffuse and direct irradiance based on field measurement. To accomplish this task, two years of diffuse and global hourly measured irradiance collected in Valencia, Spain have been analyzed. Analysis is based on one year of data, 2007, while validation is performed on an independent data set collected in 2004.

[49] The linear model assumes a constant cloud optical depth, with increasing cloud cover lowering the irradiance, while a nonlinear model applies an empirical fit to normalized direct and diffuse irradiance as a function of effective cloud cover. These two approaches exhibit high correlations in estimating hourly direct and diffuse irradiances, with R^2 above 0.95 and RMS errors of between 5.7 to 7.7 mW m^{-2}. Estimation of k_{DUV} is poorer, with an R^2 of 0.84 for both models. The nonlinear model was best in terms of overall performance.

[50] Further work is warranted to improve the prediction. In particular, detailed sky images could illustrate if the CMF_{UV} relationships shown in Figure 3 and Table 1 represent one cloud type or different types which evolve as skies become overcast. It is also of interest to examine what features of the nonlinear model are related to cloud type and cloud cover observations. These studies will lead not only to a better partitioning of the UVER, but to a better description of radiation fluxes in cloudy conditions as well.

[51] **Acknowledgments.** This research was funded by the Ministry of Science and Innovation (MICINN) of Spain through projects CGL2011–24290 and CGL2009–07790 and the Valencia Autonomous Government through project PROMETEO-2010-064. M. Núñez stayed in Valencia thanks to the Convocatòria d'estades temporals d'investigadors convidats de la Universitat de València (grant UV-ESTPC-10-24179).

References

Anton, M., J. M. Vilaplana, M. Kroon, A. Serrano, M. Parias, M. L. Cancillo, and B. A. de la Morena (2010), Empirically corrected EP-TOMS total ozone data against Brewer measurements at El Arenosillo (south western Spain), *IEEE Trans. Geosci. Remote Sens.*, *48*, 3039–3045, doi:10.1109/TGRS.2010.2043257.

Balis, D., M. Kroon, M. E. Koukouli, E. J. Brinksma, G. Labow, J. P. Veefkind, and R. D. McPeters (2007), Validation of Ozone Monitoring Instrument total ozone column measurements using Brewer and Dobson spectrometer ground-based observations, *J. Geophys. Res.*, *112*, D24S46, doi:10.1029/2007JD008796.

Bernhard, G., C. R. Booth, J. C. Ehramjian, and V. V. Quang (2009), Dissemination of data from the National Science Foundation's UV monitoring network, *Proc. SPIE Int. Soc. Opt. Eng.*, *7462*, 1–6.

Bigelow, D. S., J. R. Slusser, A. F. Beaubien, and J. H. Gibson (1998), The USDA Ultraviolet Radiation Monitoring Program, *Bull. Am. Meteorol. Soc.*, *79*, 601–615, doi:10.1175/1520-0477(1998)079<0601:TUURMP>2.0.CO;2.

Calbo, J., D. Pages, and J. A. Gonzalez (2005), Empirical studies of cloud effects on UV radiation: A review, *Rev. Geophys.*, *43*, RG2002, doi:10.1029/2004RG000155.

Commission Internationale de l'Eclairage (CIE) (1998), Erythema reference action spectrum and standard erythema dose, *ISO 17166:1999*, Vienna.

Cordero, R. R., G. Seckmeyer, D. Pisulla, L. Dasilva, and F. Labbe (2007), Uncertainty evaluation of the spectral UV irradiance evaluated using the UVSPEC radiative transfer model, *Opt. Commun.*, *276*, 44–53, doi:10.1016/j.optcom.2007.04.008.

Esteve, A. R., M. J. Marin, F. Tena, M. P. Utrillas, and J. A. Martínez-Lozano (2010), Influence of cloudiness over the values of erythemal radiation in Valencia, Spain, *Int. J. Climatol.*, *30*, 127–136.

Foyo-Moreno, I., I. Alados, F. J. Olmo, and L. Alados-Arboledas (2003), The influence of cloudiness on UV global irradiance, *Agric. For. Meteorol.*, *120*, 101–111, doi:10.1016/j.agrformet.2003.08.023.

Gao, W., D. L. Schmoldt, and J. R. Slusser (2010), *UV Radiation in Global Climate Change: Measurements, Modeling and Effects on Ecosystems*, 544 pp., Springer, New York.

Grant, R. H., and W. Gao (2003), Diffuse fraction of UV radiation in partly cloudy skies as defined by the Automated Surface Observation System (ASOS), *J. Geophys. Res.*, *108*(D2), 4046, doi:10.1029/2002JD002201.

Grant, R. H., and G. M. Heisler (2000), Estimation of ultraviolet-B irradiance under variable sky conditions, *J. Appl. Meteorol.*, *39*, 904–916, doi:10.1175/1520-0450(2000)039<0904:EOUBIU>2.0.CO;2.

Gröbner, J., G. Hülsen, L. Vuilleumier, M. Blumthaler, J. M. Vilaplana, D. Walker, and J. E. Gil (2006), Report of the PMOD/WRC-COST calibration and intercomparison of erythemal radiometers, report, PMOD-WRC, Davos, Switzerland.

Josefsson, W., and T. Landelius (2000), Effect of clouds on UV irradiance: As estimated from cloud amount, cloud type, precipitation, global radiation and sunshine duration, *J. Geophys. Res.*, *105*, 4927–4935, doi:10.1029/1999JD900255.

Kerr, J., and D. Wardle (1993), Ozone and UV monitoring program in Canada, *Proc. SPIE Int. Soc. Opt. Eng.*, *2047*, 160, doi:10.1117/12.163478.

Kneizys, F. X., E. P. Shettle, W. O. Gallery, J. H. Chetwynd Jr., L. W. Abreu, J. E. A. Selby, S. A. Clough, and R. W. Fenn (1983), Atmospheric transmittance/radiance: computer code LOWTRAN 6, *Rep. AFGL-TR-83–0187*, 197 pp., Air Force Geophys. Lab., Hanscom AFB, Mass.

Kuchinke, C., and M. Nunez (1999), Cloud transmission estimates of UV-B erythemal irradiance, *Theor. Appl. Climatol.*, *63*, 149–161, doi:10.1007/s007040050100.

Madronich, S., and S. Flocke (1997), Theoretical estimation of biologically effective UV radiation at the Earth's surface, in *Solar Ultraviolet Radiation–Modeling, Measurements and Effects*, *NATO ASI Ser.*, vol. 152, edited by C. Zerefos, pp. 23–48, Springer, Berlin.

Major, G. (1992), Estimation of the error caused by the circumsolar radiation when measuring global radiation as a sum of direct and diffuse radiation, *Sol. Energy*, *48*, 249–252, doi:10.1016/0038-092X(92)90098-U.

Martínez-Lozano, J. A., et al. (2002), UV index experimental values during the years 2000 and 2001 from the Spanish Broadband UV-B Radiometric Network, *Photochem. Photobiol.*, *76*, 181–187, doi:10.1562/0031-8655(2002)076<0181:UIEVDT>2.0.CO;2.

Mayer, B., and A. Kylling (2005), Technical note: The LibRadtran software for radiative transfer calculations—Description and examples of use, *Atmos. Chem. Phys.*, *5*, 1855–1877, doi:10.5194/acp-5-1855-2005.

McArthur, L. J. B. (2004), *Baseline Surface Radiation Network, Operations Manual*, version 2.1, 176 pp., World Clim. Res. Programme, Geneva.

McPeters, R. M., M. Krron, G. Labow, E. Brinskma, D. Balis, I. Petrovpavlovskikh, J. P. Veefkind, P. K. Bhartia, and P. F. Levelt (2008), Validation of the Aura Ozone Monitoring Instrument total ozone column product, *J. Geophys. Res.*, *113*, D15S14, doi:10.1029/2007JD008802.

Mims, F. M., and J. E. Frederick (1994), Cumulus clouds and UV-B, *Nature*, *371*(6495), 291.

Nunez, M., K. Fienberg, and C. Kuchinke (2005), Temporal structure of the solar radiation field in cloudy conditions: Are retrievals of hourly averages from space possible?, *J. Appl. Meteorol.*, *44*, 167–178, doi:10.1175/JAM-2196.1.

Nuñez, M., M. J. Marin, M. P. Utrillas, V. Estellés, and J. A. Martínez-Lozano (2010), Incorporation of aerosol effects in a clear-sky semi-empirical model of UVER radiation for Valencia, Spain, *Int. J. Climatol.*, *30*, 127–136.

Pietruczuk, A., and J. Jaroslawski (2008), An alternative method for aerosol optical thickness retrieval in the UV range, *J. Atmos. Sol. Terr. Phys.*, *70*, 973–979, doi:10.1016/j.jastp.2008.01.017.

Renaud, A., J. Staehelin, C. Frolich, R. Philipona, and A. Heimo (2000), Influence of snow and clouds on erythemal UV radiation: Analysis of Swiss measurements and comparison with models, *J. Geophys. Res.*, *105*, 4961–4969, doi:10.1029/1999JD900160.

Ricchiazzi, P., Y. Shiren, C. Gautier, and D. Sowle (1998), SBDART: A research and teaching software tool for plane-parallel radiative transfer in the Earth's atmosphere, *Bull. Am. Meteorol. Soc.*, *79*, 2101–2114, doi:10.1175/1520-0477(1998)079<2101:SARATS>2.0.CO;2.

Roy, C., P. Gies, and S. Toomey (1997), Monitoring UV-B at the Earth's surface, *Aust. Meteorol. Mag.*, *46*, 203–210.

Sabburg, J., and J. Wong (2000), The effect of clouds in enhancing UVB irradiance at the Earth's surface: A one year study, *Geophys. Res. Lett.*, *27*, 3337–3340, doi:10.1029/2000GL011683.

Schafer, J. S., V. K. Saxena, B. N. Wenny, W. Barnard, and J. J. DeLuisi (1996), Observed influence of clouds on ultraviolet-B radiation, *Geophys. Res. Lett.*, *23*(19), 2625–2628, doi:10.1029/96GL01984.

Segal, M., and J. Davis (1992), The impact of deep cumulus reflection on the ground level global irradiance, *J. Appl. Meteorol.*, *31*, 217–222, doi:10.1175/1520-0450(1992)031<0217:TIODCR>2.0.CO;2.

Shettle, E. P. (1989), Models of aerosols, clouds and precipitation for atmospheric propagation studies, *AGARD Conf. Proc.*, *454*, abstract N90-21907/15-32.

Steinmetz, M. (1997), Continuous solar UV monitoring in Germany, *J. Photochem. Photobiol.*, *41*, 181–187, doi:10.1016/S1011-1344(96)07455-6.

Thiel, S., K. Steiner, and H. K. Seldlitz (1997), Modification of global erythemally effective irradiance by clouds, *Photochem. Photobiol.*, *65*, 969–973, doi:10.1111/j.1751-1097.1997.tb07956.x.

Trevini, M. (1993), *UV-B Radiation and Ozone Depletion: Effects on Humans, Animals, Plants, Microorganisms, and Materials*, Lewis, Boca Raton, Fla.

Utrillas, M. P., M. J. Marín, A. R. Esteve, F. Tena, V. Estellés, and J. A. Martinez-Lozano (2007), Diffuse UV erythemal radiation experimental values, *J. Geophys. Res.*, *112*, D24207, doi:10.1029/2007JD008846.

Vilaplana, J. M., V. E. Cachorro, M. Sorribas, E. Luccini, A. M. de Frutos, A. Berjon, and B. de la Morena (2006), Modified calibration procedures for a Yankee Environmental Systems UVB-1 Biometer based on spectral measurements with a Brewer spectrophotometer, *Photochem. Photobiol.*, *82*, 508–514, doi:10.1562/2005-06-23-RA-590.

Weihs, P., A. R. Webb, S. J. Hutchinson, and G. W. Middleton (2000), Measurements of the diffuse UV sky radiance during broken cloud conditions, *J. Geophys. Res.*, *105*, 4937–4944, doi:10.1029/1999JD900260.

Young, G. (1963), *Statistical Treatment of Experimental Data*, 172 pp., McGraw-Hill, New York.

Zerefos, C., and A. Bais (Eds.) (1995), *Solar Ultraviolet Radiation: Modelling Measurement and Effects*, *NATO ASI Ser. I*, vol. 52, 332 pp., Springer, New York.

J. A. Martínez-Lozano and M. P. Utrillas, Solar Radiation Group, Departamento de Física de la Tierra, Universidad de Valencia, Dr. Moliner, 50 Burjassot, E-46100 Valencia, Spain. (jose.a.martinez@uv.es)

M. Nuñez, School of Geography and Environmental Studies, University of Tasmania, Churchill Avenue, Sandy Bay, Hobart, TAS 7005, Australia.